



## PLGA/PDLLA core–shell submicron spheres sequential release system: Preparation, characterization and promotion of bone regeneration in vitro and in vivo



Ying Wang<sup>a,b,1</sup>, Yan Wei<sup>a,f,1</sup>, Xuehui Zhang<sup>d</sup>, Mingming Xu<sup>a</sup>, Feng Liu<sup>b</sup>, Qi Ma<sup>a</sup>, Qing Cai<sup>c,\*</sup>, Xuliang Deng<sup>a,e,f,\*</sup>

<sup>a</sup> Department of Geriatric Dentistry, Peking University School and Hospital of Stomatology, Beijing 100081, PR China

<sup>b</sup> First Clinical Division, Peking University School and Hospital of Stomatology, Beijing 100034, PR China

<sup>c</sup> Beijing Laboratory of Biomedical Materials and State Key Laboratory of Organic-Inorganic Composites, Beijing University of Chemical Technology, Beijing 100029, PR China

<sup>d</sup> Department of Dental Materials, Peking University School and Hospital of Stomatology, Beijing 100081, PR China

<sup>e</sup> National Engineering Laboratory for Digital and Material Technology of Stomatology, Beijing 100081, PR China

<sup>f</sup> Department of Prosthodontics, Peking University School and Hospital of Stomatology, Beijing 100081, PR China

### HIGHLIGHTS

- A way to electrosprayed core–shell submicron spheres in one step was found.
- VEGF and BMP-2 were successfully encapsulated in core–shell submicron spheres.
- A sequential release of VEGF and BMP-2 was achieved.
- Sequential release of VEGF and BMP-2 could promote rat bone defect healing.

### ARTICLE INFO

#### Article history:

Received 12 December 2014

Received in revised form 19 February 2015

Accepted 14 March 2015

Available online 27 March 2015

#### Keywords:

Sequential release

Core–shell submicron spheres

Bone regeneration

BMP-2

VEGF

### ABSTRACT

Core–shell polymer spheres of submicron diameter are a promising vehicle for sequential delivery of angiogenic and osteogenic growth factors to bone defect sites, to simulate the orchestrated temporal sequence of angiogenesis and osteogenesis. To achieve a homogeneous distribution pattern in the scaffold matrix and avoid fast biological clearance in vivo, attention should be paid to the particle size of the spheres, using a modified coaxial electrospraying technique, we prepared core–shell spheres about 1  $\mu\text{m}$  in diameter using the polymers poly-(D,L-lactide) in the shell and poly(L-lactide-co-glycolic acid) in the core, and loaded them with VEGF and BMP-2, growth factors that stimulate angiogenesis and osteogenesis, respectively. PLGA/PDLLA controlled sequential delivery profiles, including an initial burst release of VEGF and a sustained release behavior of BMP-2 from the VEGF//BMP-2 spheres, were obtained. The VEGF and BMP-2 released from the spheres maintained their bioactivity; VEGF could enhance the proliferation of endothelial cells and BMP-2 could promote the osteogenic differentiation of bone marrow mesenchymal stem cells. Micro-computed tomography analysis showed that, among all the experimental groups, implantation of VEGF//BMP-2 spheres into rat cranial critical-sized bone defects enhanced new bone formation to the greatest extent, resulting in the largest amount of new bone volume and the largest isolated bone islands. Histological examination showed that VEGF//BMP-2 spheres also significantly increased in-growth of blood vessels with positive CD31 staining. All these findings suggest that the submicron-scale core–shell VEGF//BMP-2 spheres developed in this study are capable of yielding sequentially coupled angiogenesis and osteogenesis, implying their extensive application in bone tissue regeneration.

© 2015 Elsevier B.V. All rights reserved.

\* Corresponding authors at: Department of Geriatric Dentistry, Peking University School and Hospital of Stomatology, Beijing 100081, PR China (X. Deng). Tel.: +86 10 82195637; fax: +86 10 62179977x5581.

E-mail addresses: [caiqing@mail.buct.edu.cn](mailto:caiqing@mail.buct.edu.cn) (Q. Cai), [kqdengxuliang@bjmu.edu.cn](mailto:kqdengxuliang@bjmu.edu.cn) (X. Deng).

<sup>1</sup> These authors contributed equally to this work.

## 1. Introduction

The repair of large bone defects remains a major challenge in orthopedic and maxillofacial surgery. To avoid the potential disadvantages of autografts and allografts [1], artificial bone substitutes have been proposed as promising alternatives in clinical applications [2,3]. However, controversy has continued regarding their clinical outcomes in bone defect repair. There have been reports that the rate of bone regeneration after implantation of bone substitutes cannot meet expectations and may require additional surgery [4]. Currently, the critical strategy in designing bone defect fillings is to mimic the procedure of natural bone healing [5–8]. In light of the complex and highly coordinated temporal process in natural bone development and defect regeneration, angiogenesis has been considered not only a prerequisite to ossification but also necessary for bone morphogenesis [9–12]. Therefore, scaffolds that simulate the temporal coupling of angiogenesis and osteogenesis may promote bone defect repair.

Various scaffolds have been developed that gradually release growth factors (GFs) to orchestrate angiogenesis and osteogenesis [3,13,14]. Different kinetic delivery patterns were obtained by incorporating different GFs in either the inner or outer spatial structure of scaffolds, or by altering the degradability of blended biomaterial components loaded with distinct GFs [15]. Several types of encapsulating techniques have been developed including supercritical CO<sub>2</sub> mixing [16], hydrogel fiber entrapment [17], and microsphere encapsulation [18–22], to achieve temporal release of different GFs. These methods can also provide a protective shell to avoid possible reciprocal interactions between different GFs in direct contact. Considering their versatile administration methods, and the ease with which they can be incorporated within numerous scaffold matrices, core-shell spheres are among the most attractive options for sequentially delivering GFs.

Choi et al. have reported the fabrication, via electrodropping, of core-shell spheres consisting of poly(L-lactide-co-glycolic acid) (PLGA) as the core and alginate as the shell [22]. The diameter of these spheres was  $412 \pm 83 \mu\text{m}$ . Chang et al. prepared poly(D,L-lactide)(PDLLA)/PLGA core-shell spheres with diameters around  $15 \pm 1.6 \mu\text{m}$  through co-axial electrohydrodynamic atomization [18]. Meanwhile, Cao et al. obtained nanoscale (275–860 nm) poly-lactide-b-polyethylene glycol (PLA/PEG) core-shell spheres by co-axial electrospinning [23].

Particle sizes should be seriously taken into account in regenerative medicine because this parameter might play a critical role in determining the translation from bench to clinical applications [24]. Large spheres have the innate disadvantage of being able to lodge within scaffolds, especially those with complex porous three-dimensional structure, thus losing the homogeneous distribution of encapsulated factors in matrix or tissues. Nanoscale spheres might be readily endocytosized by surrounding cells [25], thus limiting their residence time in the implantation area and weakening their biological effects. Considering these issues, we speculate that core-shell submicron-sized spheres might be inspiring candidates for sustained timely release of angiogenic and osteogenic factors to achieve synergistic therapeutic effects by mimicking the synchronized balance of angiogenesis-osteogenesis in bone formation.

In this work, PLGA-BMP-2/PDLLA-VEGF core-shell submicron-spheres about  $1 \mu\text{m}$  in diameter were fabricated by a modified electrospinning technique. VEGF, which boosts angiogenesis, was loaded in the PDLLA outer layer to be released first. BMP-2 was incorporated in the core part of PLGA to enhance successive osteogenesis. The release characteristics of VEGF and BMP-2 from

these submicron-sized spheres were examined, along with the corresponding bioactivity of release factors on the proliferation of microvascular epithelial cells (MECs) and the osteogenic differentiation of bone marrow stem cells (BMSCs) were investigated. Furthermore, the coupling of angiogenesis-osteogenesis in rat critical-sized calvarial bone defect repair via PLGA-BMP-2/PDLLA-VEGF core-shell submicron-spheres implantation was evaluated.

## 2. Methods and materials

### 2.1. Materials

PLGA with a lactide-glycolide molar ratio of 75:25 (*M<sub>w</sub>*, 10 kDa) was obtained from Birmingham Polymers (Birmingham, AL, USA). PDLLA (*M<sub>w</sub>*, 10 kDa) was obtained from the Institute of Shandong Biomedical Instruments (Shandong, China). Organic solvents 2,2,2-trifluoroethanol (TFE) (purity 99.9%) were supplied by Sinapharm Chemical Reagent Beijing Co., Ltd. (Beijing, China) and used directly. Phosphate-buffered saline (PBS; pH 7.4) was purchased from Beijing Zoman Biotechnology Co., Ltd. (Beijing, China). Rat BMSCs, MECs, and alizarin red stain kit were obtained from the Cyagen Biosciences Inc. (Guangzhou, China). Cell Counting Kit (CCK-8) was purchased from the Beyotime Institute of Biotechnology (Haimen, China). The rat BMP-2, VEGF ELISA kit, and alkaline phosphatase (ALP) assay kit were supplied by Sigma Aldrich Inc. (St. Louis, MO, USA).

### 2.2. Coaxial electrospinning

Different formulas were prepared, to decide upon the appropriate concentration of polymer for core and shell solutions. The distance between tips of nozzle and collection platform was set as 20 cm. Using an applied voltage of 15 kV and a total flow rate of 0.8 mL/h for electrospinning, the concentration of core solution was set at 4% w/v and various concentrations of the shell solution were prepared: 1%, 2%, 3%, and 4% w/v. Scanning electron microscopy (SEM; S-3000N, Hitachi, Japan) was employed to determine the appropriate concentration that could generate smooth spheres. After this concentration had been identified, the mixtures were subjected to different core-shell flow ratios (1:1, 1:2, 1:3, and 1:4) during electrospinning, followed by imaging via transmission electron microscopy (TEM; H-7650B; Hitachi Global, Japan) to determine the appropriate flow ratio that could generate spheres with core-shell structure. The diameters of the submicron spheres were calculated as the average for approximately 150 spheres, upon analyzing the images with Image J software (National Institutes of Health, Bethesda, MD, USA).

BMP-2 was dissolved in deionized water at a specified concentration, and the aqueous solution was mixed into PLGA/TFE solution to obtain the core solution. VEGF was dissolved in deionized water and then mixed into the shell solution of PDLLA/TFE. Coaxial electrospinning was conducted by a compound nozzle, with the solutions for the core and the shell being delivered to the coaxial core and shell needles. The exit orifice diameters of the core and shell capillaries were 0.5 mm and 0.8 mm, respectively. Electrospun submicron spheres were collected on a plate covered with aluminum foil. They were freeze dried for 1 day before further characterization. In this manner, four types of submicron spheres were fabricated by electrospinning: PLGA-BMP-2/PDLLA-VEGF spheres (VEGF//BMP-2 group, VEGF in the shell, and BMP-2 in the core); PDLLA-VEGF/PLGA spheres (VEGF group, containing only VEGF in the shell); PLGA/PDLLA-BMP-2 spheres

(BMP-2 group, containing only BMP-2 in the core); and blended PDLLA–PLGA spheres (VEGF&BMP-2 group, both the PDLLA core and PLGA shell contained both VEGF and BMP-2).

### 2.3. *In vitro* release study

To investigate *in vitro* release from the particles, 3 mL 0.01 M PBS (pH 7.4) was added to a sealed vial containing 50 mg submicron spheres, and the system was maintained with shaking at 65 rpm at 37 °C for different amounts of time. At each time point, all the liquid was removed by centrifugation and the vial was refilled with 3 mL fresh PBS. The GFs concentration in the supernatant was analyzed by ELISA. For each group, the assay samples were taken in triplicate at each time interval. And the release behavior were presented by percentage [26].

### 2.4. Cell growth examination

The *in vitro* activity of released VEGF was determined by its proliferative effects on MECs. Five hundred milligram submicron spheres were incubated with rat MECs in 5 mL 0.01 M PBS at 65 rpm at 37 °C and the PBS was collected and refreshed every 24 h. After 28 days, all of the collected PBS was freeze dried and re-dissolved in cell culture medium obtaining a VEGF concentration of 10 ng/mL [27]. The cells were seeded into a 24-well tissue culture plate (Falcon) with a starting density of 20,000 cells/cm<sup>2</sup> and sub-cultured in DMEM (Gibco, Paisley, UK) containing 10% FBS (Gibco, Paisley, UK) and 1% penicillin/streptomycin (Sigma-Aldrich). The samples were then incubated at 37 °C in a humidified atmosphere with 5% CO<sub>2</sub>. The cell growth level was assessed by the CCK-8 kit (Dojindo, Japan) at days 1, 3, and 7.

### 2.5. ALP activity test and alizarin red staining

The bioactivity of the released BMP-2 was examined by its ability to induce osteogenesis of BMSCs. Osteoblastic differentiation of the BMSCs was observed by measuring the production of ALP. One thousand milligram submicron spheres were incubated with 5 mL 0.01 M PBS water at 65 rpm at 37 °C, and the PBS supernatant was collected and refreshed every 24 h. After 28 days, all the collected PBS was freeze dried and re-dissolved by cell culture medium obtaining a BMP-2 concentration of 100 ng/mL [28]. BMSCs were cultured at 37 °C in a humidified atmosphere with 5% CO<sub>2</sub>. They were assessed using an ALP activity kit at 7 and 14 days. At day 21, the BMSCs were tested by alizarin red staining. Triplicate samples in each group were used for all cellular tests.

### 2.6. Real-time PCR

BMSCs were collected at 7 days and their RNA was extracted using the RNeasy Mini Kit (Qiagen, Valencia, CA, US). The RNA

**Table 2**

The primer sequences of osteogenic genes ALP, OCN, and BMP-2.

GGTCGGTGTGAACGGATTGG	Rat GAPDH F
GCCGTGGGTAGAGTCATACTGGAAC	Rat GAPDH R
CACCAACGTGGCCAAGAACAT	Rat ALP F
AGGGGAAGTGTCCATCTCCA	Rat ALP R
TGCTCAGCTTCCATCACGAAG	Rat BMP2 F
TCTGGAGCTCTGCAGATGTGA	Rat BMP2 R
GACCCCTCTCTGCTCACTCTG	Rat OCN F
GCTCCAAGTCCATTGTTGAGG	Rat OCN R

concentration was determined spectrophotometrically at 260 nm using a NanoDrop ND-2000 Spectrophotometer (Thermo Fisher Scientific, Wilmington, DE). One milligram of RNA was used to synthesize cDNA with the First Strand cDNA Synthesis Kit (Gene Copoeia Inc., USA) according to the manufacturer's instructions. ABI PRISM 7500 Real-Time PCR System (Applied Biosystems, Foster City, CA, USA) were used to perform quantitative real-time PCR. The amplifications were performed in triplicate with the following PCR conditions: 1 cycle at 95 °C for 30 s, and 45 1-min cycles at 60 °C for 30 s followed by 72 °C for 30 s. The primer sequences of osteogenic genes ALP, OCN, and BMP-2 are listed in Table 1. The data were analyzed with the 2(-ddct) method [29] (see Table 2).

### 2.7. *In vivo* implantation procedure in rat calvarium

Twenty-four 10-week-old male Sprague-Dawley rats were used in this study. The animals were sacrificed 2, 4, and 8 weeks after implantation. At each time point, 5 groups were divided according to the samples produced, which were untreated group, VEGF group (filled with sample A in Table 1), BMP-2 group (filled with sample B in Table 1), VEGF&BMP-2 group (filled with sample C in Table 1) and VEGF//BMP-2 group (filled with sample D in Table 1). To make sure there were 3 samples for each group, 8 rats were sacrificed at each time point. The animal surgery protocol was performed in accordance with the Animal Care and Use Committee of Peking University. The animals were anesthetized by means of abdominal cavity injection using pelltobarbitalum natricum (40 mg/kg). The skin hair on the cranium was shaved and the surgical region was aseptically treated using povidone-70% ethanol. A 15-mm skin incision was made and the periosteum was elevated for trephining. Two critical-sized full-thickness bone defects (5-mm diameter) were prepared in each rat at the center of each parietal bone using a saline-cooled trephine drill. Care was taken not to damage the underlying sagittal sinus and dura matter. According to loading efficiency, about 1.5 µg VEGF particles or/and 3 µg BMP-2 were set for each defect. Each defect was randomly implanted with one of the four types of submicron-sized spheres encapsulated by gelatin or kept empty as a negative control, Fig. 1. To prepare samples for testing, the skin was removed and the cranioaural

**Table 1**

Preparation parameters of coaxial electrospray used in this study.

Sample	Compositions				Flow rate (ml/h)		Loading efficiency(%)		Collection distance (cm)	Voltage (kV)
	Core solution (2 mL)		Shell solution (6 mL)		Core	Shell	BMP-2	VEGF		
	BMP-2(µg)/DI water	PLGA/TFE (w/v%)	VEGF(µg)/DI water	PLDL/TFE (w/v%)						
A group (VEGF)	0	4	3	2	0.2	0.6	none	72.66 ± 2.60	20	15
B group (BMP-2)	6	4	0	2	0.2	0.6	85.42 ± 3.74	none	20	15
C group (VEGF&BMP-2)	Mixed by solutions as D group core and shell solution				0.8		79.69 ± 1.71	80.09 ± 1.72	20	15
D group (VEGF//BMP-2)	6	4	3	2	0.2	0.6	84.75 ± 2.12	74.91 ± 4.39	20	15

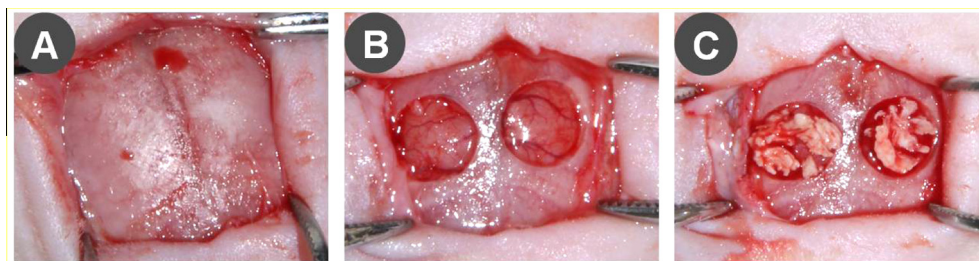


**Fig. 1.** Animal surgery process: a 15-mm skin incision was made and the periosteum was elevated (A), two critical-sized full-thickness bone defects (5-mm diameter) were prepared (B), implanted submicron-sized spheres encapsulated by gelatin in corresponding defect (C).

samples with surrounding tissues were withdrawn en bloc and fixed in 10% neutral buffered formalin solution for 24 h at room temperature.

### 2.8. Micro-CT analysis

Micro-CT (INVEON MM. CT 3121, SIEMENS, USA) was used to observe the formation of new bone within the defect region. The harvested specimens were scanned, with each frame exposed for 20 ms. Scanning was performed in a direction parallel to the coronal aspect of the calvarial bone surrounding the defect area. A cylindrical region of interest (ROI) was precisely positioned over the center of each defect, encompassing all new bone within the defect site. Micro-CT images were reconstructed over the ROI using COBRA Exxim (SIEMENS, USA) and the data was analyzed by Inveon Research Workplace (SIEMENS, USA). The total volume of newly formed bone within the ROI was measured using three-dimensional images by assigning a threshold for total bone content (including trabecular and cortical bone) and subtracting any contribution from the scaffold (determined previously). Three samples for each group were measured and their total volume of bone was reported in  $\text{mm}^3$ .

### 2.9. Histomorphometry

For histomorphometric analysis, the fixed samples were decalcified, dehydrated, and embedded in paraffin, then serially sectioned with a microtome (LEICA) at  $2\ \mu\text{m}$  thickness and finally mounted on microscope slides. Slides with tissue sections were deparaffinized and dehydrated with xylene and an ethanol series. The slides were stained with hematoxylin and eosin and immunohistochemical staining and examined using a light microscope (CX21, Olympus, Japan).

### 2.10. Statistics

Statistical analyses were performed using the SPSS 19.0 software (Chicago, IL) and all quantitative data were expressed as mean standard deviation (SD). Statistical differences were determined using Student's *t* test for independent samples. Differences

between groups of  $*p < 0.05$  were considered statistically significant and  $**p < 0.01$  was considered highly significant.

## 3. Results

### 3.1. Production and characterization of submicron spheres

SEM observation revealed that smooth core-shell microspheres were achieved only with core-shell polymer concentrations of 4% w/v PLGA and 2% w/v PDLLA, respectively (Fig. 2b). Below this concentration, at 4% w/v PLGA and 1% w/v PDLLA, microspheres with collapsed structure were obtained (Fig. 2a). When the polymer concentrations increased to 4% w/v PLGA and 3% w/v PDLLA (Fig. 2c) and 4% w/v-PLGA and 4% w/v PDLLA (Fig. 2d), relatively larger and heterogeneous microspheres with fibers were achieved.

As for the flow rate, it was observed that only a core-shell flow rate ratio of 1:3 resulted in a narrow size distribution of smooth spheres with clear core-shell structure and diameter about  $1\ \mu\text{m}$  (Fig. 3c). Some particles with ambiguous core-shell structure were achieved with a core-shell flow rate ratio of 1:2 (Fig. 3b). When this ratio decreased to 1:4 (Fig. 3d) or increased to 1:1 (Fig. 3a), certain particles without core-shell structures were generated (see Table 3).

Thus the concentrations of 4% w/v PLGA and 2% w/v PDLLA and a core-shell flow rate ratio of 1:3 were set to produce core-shell microspheres for in vivo experiment. As shown in Table 1, four samples were generated and characterized by SEM, TEM and diameter analysis (Fig. 4). Particles with smooth surface and core-shell structure were produced. And the core-shell structure was also confirmed by Laser scanning confocal microscopy in our previous study [30]. The diameter of A, B, C, D group was about  $0.7\ \mu\text{m}$  and showed a narrow size distribution ranged from  $0.2\ \mu\text{m}$  to  $2.0\ \mu\text{m}$ . And the diameter of the four groups' particles were statistically insignificant between each group ( $*p < 0.05$ ).

### 3.2. In vitro release profiles of growth factors

The schema graphs show the distribution of microstructure and growth factors in the four types of submicron spheres (Fig. 5A). The corresponding cumulative release kinetics indicated that a

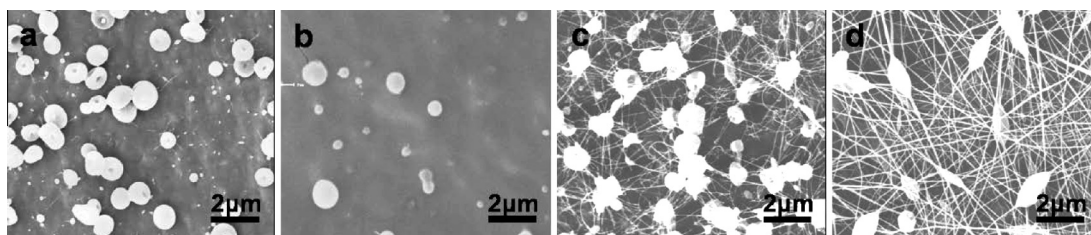


**Fig. 2.** SEM Morphology of the submicron spheres fabricated by coaxial electrospinning under core/shell polymer concentrations of 4% w/v PLGA and 1% w/v PDLLA (a), 4% w/v PLGA and 2% w/v PDLLA (b), 4% w/v PLGA and 3% w/v PDLLA (c), and 4% w/v PLGA and 4% w/v PDLLA (d).

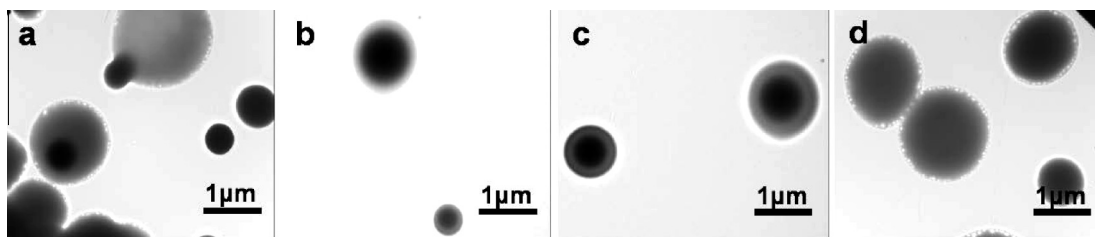


Fig. 3. TEM microstructures of the submicron spheres fabricated by coaxial electrospinning under core/shell flow ratios of (a) 1:1, (b) 1:2, (c) 1:3, and (d) 1:4.

Table 3

Preparation parameters for samples in Figs. 2 and 3 used in this study.

Sample	Compositions				Core/Shell flow ratio		Collection distance (cm)	Voltage (kV)
	Core solution		Shell solution		Core	Shell		
	BMP-2 ( $\mu\text{g}$ )/DI water	PLGA/TFE (w/v%)	VEGF ( $\mu\text{g}$ )/DI water	PLDL/TFE (w/v%)				
Fig. 2a	6	4	3	1	1	1	20	15
Fig. 2b	6	4	3	2	1	1	20	15
Fig. 2c	6	4	3	3	1	1	20	15
Fig. 2d	6	4	3	4	1	1	20	15
Fig. 3a	6	4	3	2	1	1	20	15
Fig. 3b	6	4	3	2	1	2	20	15
Fig. 3c	6	4	3	2	1	3	20	15
Fig. 3d	6	4	3	2	1	4	20	15

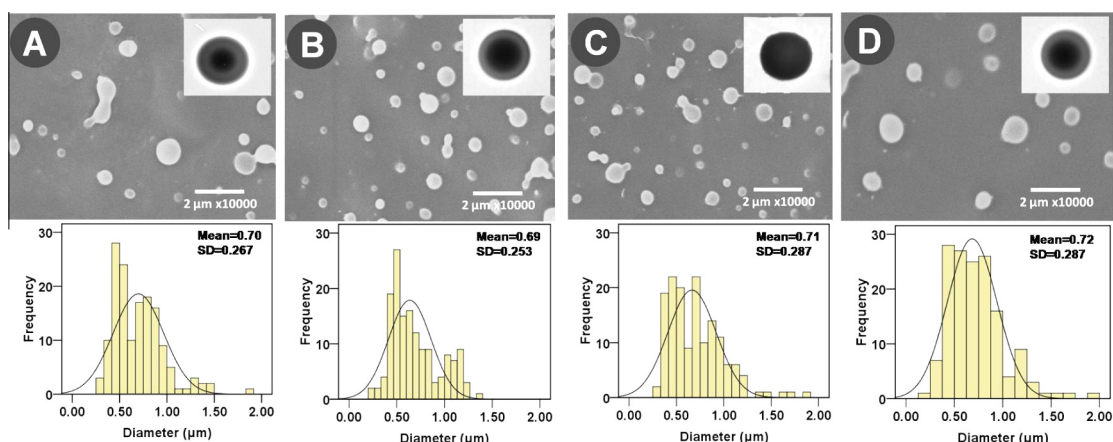


Fig. 4. SEM Morphology, TEM microstructures and the diameter analysis of the submicron spheres.

sequential delivery pattern was achieved in groups of VEGF//BMP-2 (Fig. 5B d and h), whereby the VEGF in the shell was delivered by an initial burst release and nearly 80% of VEGF was released within the first 10 days, while BMP-2 in the core displayed relatively stable release behavior over time. The VEGF group exhibited a similar release profile (Fig. 5B a and e) as its counterpart in the VEGF//BMP-2 group, and likewise for the BMP-2 release profile of BMP-2 group (Fig. 5B b and f). The VEGF&BMP-2 group showed burst release of VEGF and BMP-2 within the first 3 days, and stable release in the later following stages (Fig. 5B c and g).

### 3.3. In vitro bioactivity of released growth factors

The release of VEGF into the endothelial cell culture medium from the core-shell sub-micron spheres significantly increased the proliferation of MECs in culture after 3 days (Fig. 6A). An obvious enhancement in alkaline phosphatase production and matrix mineralization was visualized by ALP and Alizarin Red S

staining of BMSCs seeded in medium contained BMP-2 released from submicron spheres (Fig. 6C). Furthermore, the mRNA expression levels of all selected osteogenic genes, including ALP, OPN, and BMP-2, were significantly enhanced in BMSCs cultured in BMP-2 release medium at the 14th day (Fig. 6B).

### 3.4. Micro-CT analysis

Representative three-dimensional morphological  $\mu$ -CT scanning images indicated the extent of new bone formation in rat calvarial bone defects after 2, 4, and 8 weeks post-operation (Fig. 7). Qualitatively, the healing capacity of VEGF//BMP-2 group was most significantly enhanced among all the groups at all time points (Fig. 7A e, j and o). Over the study duration, the untreated control group remained primarily empty (Fig. 7A a, f and k), indicating that critically sized calvarial defects were not able to self-heal. At 2 weeks, small amounts of mineralized tissue predominantly located at the defect periphery were observed in all experimental groups (Fig. 7A

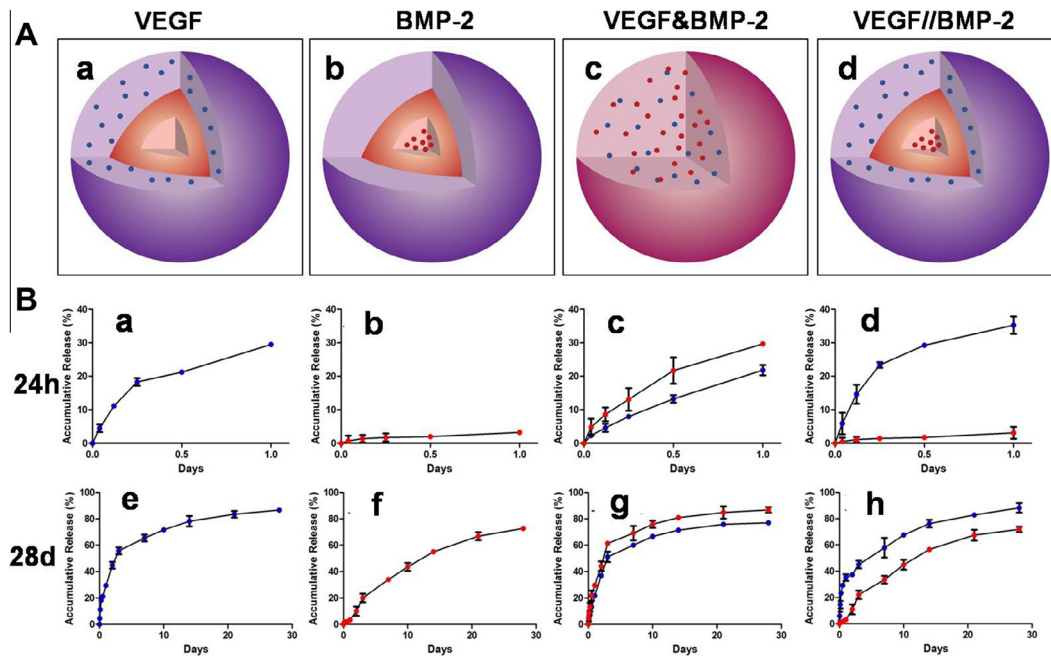


**Fig. 5.** (A) Schema graphs for samples in group A (a, only with VEGF in shell), B (b, only with BMP-2 in shell), C (c, with both VEGF and BMP-2 but without core-shell structure), D (d, with both VEGF in shell and BMP-2 in core). (B) Release kinetics of growth factors in A, B, C, D groups over time periods of 24 h (a, b, c, d) and 28 days (e, f, g, h). Blue spots represent VEGF and red spots represent BMP-2. (For interpretation of the references to color in this figure legend, the reader is referred to the web version of this article.)

b–e), but mineralized spicules were only seen in the VEGF//BMP-2 group (Fig. 7A e). The defect areas gradually decreased as the border shrunk centripetally. After 4 weeks of healing, the largest amount of new plate-like-pattern bone at peripheral defect sites was seen in the VEGF//BMP-2 group (Fig. 7A j). When compared with the VEGF group (Fig. 7A g), more bone was observed in VEGF&BMP-2 (Fig. 7A i) and BMP-2 (Fig. 7A h) groups. This trend continued and differences among groups were likewise significant at the end of this experiment (Fig. 5A k–o). Noticeably, some plate-like trabeculae appeared in the middle area of the bone defect in the VEGF//BMP-2 group after the 8-week healing period (Fig. 7A o).

In correlation with the image observation, the three-dimensional micro-architectural parameter of bone volume (BV) was assessed as a quantitative indicator of new bone formation (Fig. 5B). Consistent with the results achieved by direct qualitative comparison, the highest BV values were observed in the VEGF//BMP-2 group at all the preset time points. The VEGF&BMP-2 group resulted in slightly higher BV values compared with the BMP-2 group, which was followed by the VEGF group. The untreated group had the lowest BV value among all groups.

### 3.5. Histological observation and immunohistochemical assessment

No inflammation or necrosis was observed in all animals. During the study period, defects in the untreated controls were sparsely populated with fibrous tissue but no appreciable bone formation, along with a clear boundary of native bone (Fig. 8a1, a2, f1, f2, k1, k2). Instead of self-healed bone, marrow-like tissue gradually filled the defect areas in all experimental groups over the study duration. As compared with untreated controls (Fig. 8a1, a2, f1, f2, k1, k2), some less organized new bone tissue was observed at the periphery of defect sites in the VEGF and BMP-2 groups. Meanwhile, the VEGF&BMP-2 group displayed a large amount of bone tissue and mineralized matrix deposition at the periphery and in the center of defect sites (Fig. 8d1, d2, i1, i2, n1, n2). The

sequentially-releasing VEGF//BMP-2 group showed the most advanced formation of new bone, leaving an indistinguishable boundary between native bone and regenerated bone tissue (Fig. 8e1, e2, j1, j2, o1, o2). In addition, the histological evaluation also revealed that the highest activity of blood vessel in-growth appeared in the VEGF//BMP-2 group, followed by the VEGF&BMP-2, BMP-2, VEGF, and untreated groups.

Immunostaining of CD31, a marker of newly formed blood vessels, reveals a continuous increase of blood vessel in-growth into the defect areas as implantation time was increased in all groups (Fig. 9A). The sequentially releasing VEGF//BMP-2 group yielded the highest activity of angiogenesis (Fig. 9B). At 8 weeks post-implantation in the VEGF//BMP-2 group, plenty of blood vessels were randomly dispersed within the defect area and even mature nascent marrow cavities were observed (Fig. 9A e, j and o). The combined-release group VEGF&BMP-2 showed more in-growth of new blood vessels (Fig. 9A d, i and n) than the singly-releasing VEGF and BMP-2 groups. The untreated group showed the least activity of vascularization.

The calculated number of vascular sections for the VEGF//BMP-2 and VEGF&BMP-2 groups were not significantly different at 2 weeks post-implantation, but were significantly higher than VEGF and BMP-2 groups (Fig. 9B). The sequentially releasing VEGF//BMP-2 group retained a larger number of capillaries than the combined-releasing VEGF&BMP-2 group at 4 and 8 weeks post-implantation. Although the single releasing VEGF group yielded a significant higher numbers of new blood vessels than the BMP-2 group at 2 weeks post-implantation, these two groups displayed similar moderate vascular numbers at later two time points. The untreated group exhibited the least amount of new blood vessels at all time points.

Immunohistochemical markers including OCN were qualitatively detected under light microscopy from sections of the defects in all groups, indicating an increase in bone matrix deposition and maturation of active bone-forming sites. Although OCN was positively expressed within all groups, the greatest intensity

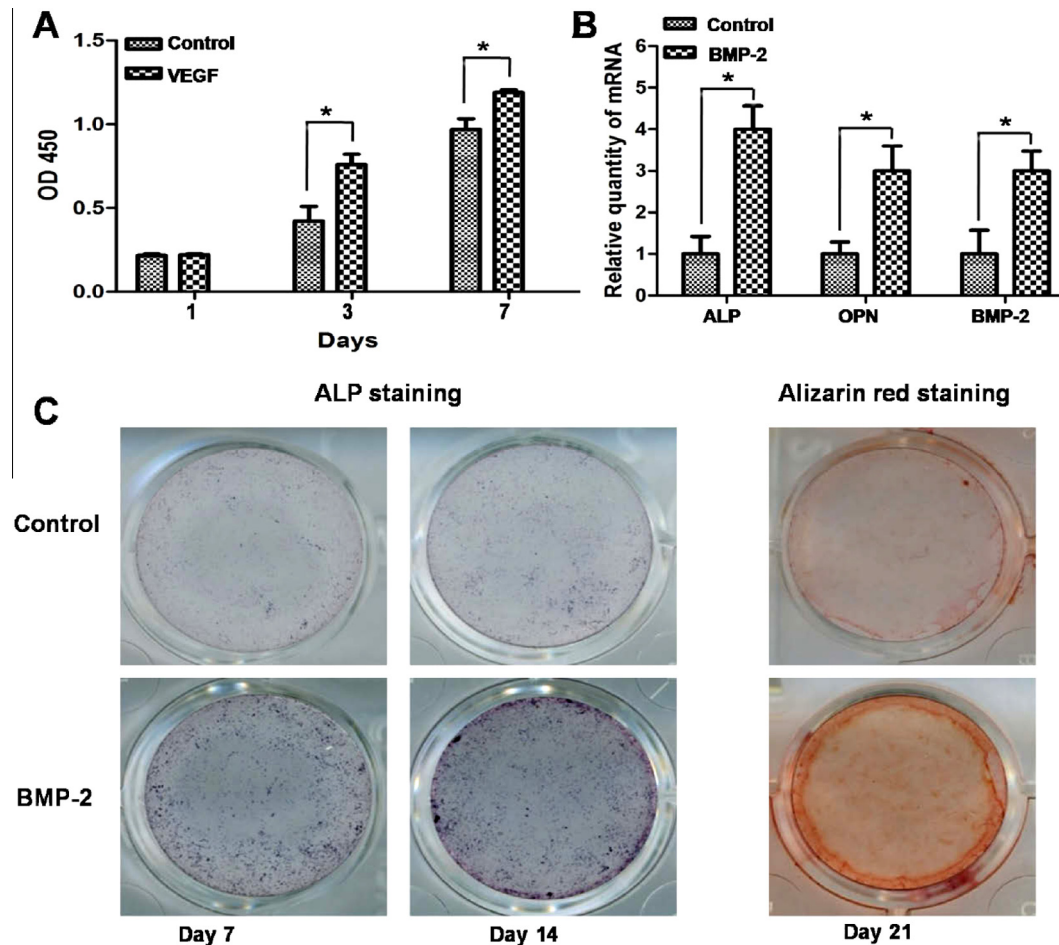


**Fig. 6.** In vitro bioactivity of VEGF and BMP-2 released from core-shell submicron spheres. (A) Cell proliferation of MECs cultured in medium contained VEGF released from core-shell submicron spheres. (B) Osteogenic differentiation of BMSCs cultured in medium contained BMP-2 released from submicron spheres. (a) The ALP staining at the 7th and 14th day and Alizarin Red S staining at the 21st day. (b) Gene expression profiles of ALP, OPN, and BMP-2 analyzed by RT-qPCR at the 14<sup>th</sup> day. Cells cultured in standard medium were set as the control groups (\* $p < 0.05$ ).

of staining and largest staining area at all time points was observed within the VEGF//BMP-2 group at all time points (Fig. 10e, j and o), followed by the VEGF&BMP-2, BMP-2, VEGF, and untreated groups.

#### 4. Discussion

Combining multiple essential GFs with coordinated release kinetics offers a promising strategy to enhance bone regeneration through simulating the spatial-temporal signaling cascades involved in natural bone development and spontaneous healing [7,31–33]. Although core-shell spheres have showed great potential in facilitating sequential release of GFs [22,34,35], their size must be taken into account when considering their translation from bench to clinical use because of the narrow size window of core-shell capsules for use in complex in vivo environments [25]. In this work, PLGA-BMP-2/PDLLA-VEGF core-shell submicron-spheres about 1  $\mu\text{m}$  in diameter were successfully fabricated by co-axial electrospinning. VEGF was loaded in the PDLLA shell, and BMP-2 was incorporated into the PLGA core. The GFs bioactivity was well maintained throughout the manufacturing process. Sequential release of VEGF and BMP-2 was achieved. Synchronized angiogenesis and osteogenesis was observed in the repair of a critical-sized bone defect in rat cranium upon introducing the particles.

Among the various microencapsulating techniques for making core-shell spheres, including emulsion-solvent evaporation [36],

electrohydrodynamic atomization [18], electrodropping [22], and self-assembly [37], coaxial electrospinning has advantages in preserving the structural integrity, narrowing the particle size distribution, and maintaining the bioactivity of loaded proteins [23,25,38–40]. Chang et al. have successfully produced a hollow microsphere with a single hole in its shell by coaxial electrohydrodynamic atomization (CEHDA). In their study, Polymethylsilsesquioxane (PMSQ) was used as a model shell material encapsulating a core of a volatile liquid, perfluorohexane (PFH), which was subsequently evaporated to produce the hollow microspheres. But the microspheres' ability of GFs encapsulation were not explored [18]. Another research also produced core-shell microcapsules by PLGA and alginate. This study focus on the initial burst release controlling. And they found that the use of high-molecular-weight PLGA (HMW 270 000) restrains the initial burst release of protein compared to that of low-MW PLGA (LMW 40 000). Layer-by-layer (LBL) assembly of chitosan and alginate on MCs is also useful in controlling the release profile of biomolecules but made the production process more complicated [22]. This study produced nanosized PLA-PEG particles with a core-shell structure by coaxial tri-capillary electrospinning-template removal process. The nanoparticles exhibited sustained release of paclitaxel for more than 40 days. But the location of the paclitaxel in the nanoparticles, i.e., in the core or shell layer, did not have a significant effect on its release [23,25,38–40]. And most electrospun spheres in the past have had sizes in the supra-micron

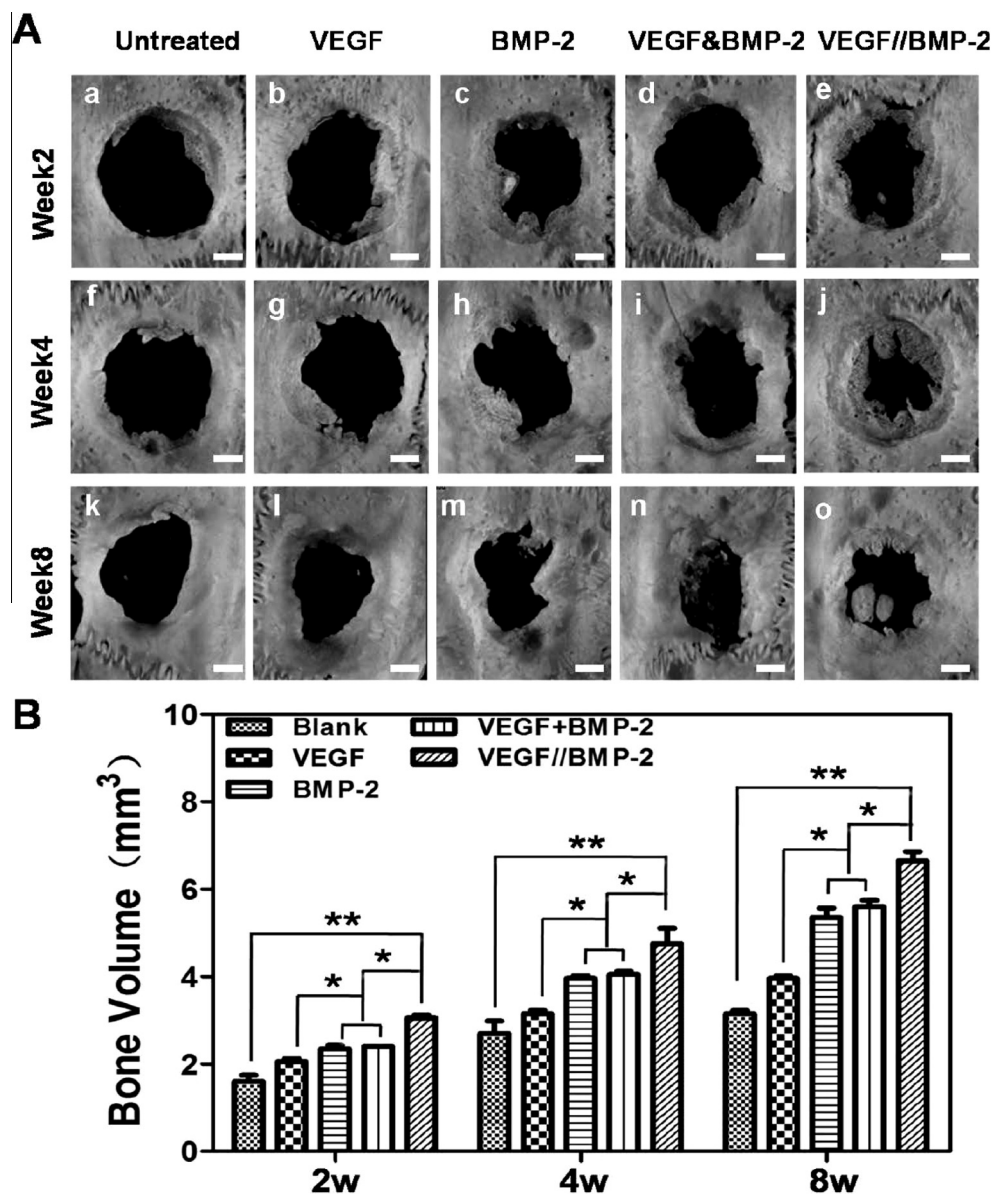


**Fig. 7.** (A) Representative 3D  $\mu$ -CT images of repaired rat calvarial bone defects at (a) 2th, (b) 4th, and (c) 8th weeks post-implantation. (B) Quantitative analysis of bone volume at 2nd, 4th, and 8th weeks post-implantation. Scale bar = 1 mm. (\* $p < 0.05$  and \*\* $p < 0.01$ ).

or nanometric scale, resulting in specific size-dependent biological influence [25]. So how to obtain a core-shell structure particles in a simple way and have the ability to achieve a sequential release of two drugs was very important. To address this issue, the present study used several strategies to fabricate core-shell spheres approximately 1  $\mu$ m in size by co-axial electrospinning. In the fabricating process, the major factor in maintaining appropriate core-shell structure is the balance among the electrostatic repulsion (determined by the applied voltage), surface tension, viscoelastic force (determined by the polymer concentration of solution), and flow rate. A previous study from our group reported the production of PLGA core-shell microspheres with a mean diameter of 2.45  $\mu$ m [30]. Here, PDLLA with stronger polarity and electroconductivity was used to replace PLGA in the shell because of the ease with which its biodegradation can be regulated. By electrospinning with an applied voltage of 15 kV and a total flow rate of 0.8 mL/h, smooth core-shell microspheres were obtained with polymer concentrations of 4% w/v PLGA and 2% PDLLA. When the PDLLA concentration increased, relatively larger and

heterogeneous microspheres appeared. This may be because the microspheres made from solutions of higher polymer concentration contain less solvent, which results in a smaller mass loss owing to evaporation during electrospinning. At lower concentrations, although the mean diameter of the spheres was smaller, the core-shell structure collapsed after the solvent evaporated. As for flow rate, it was observed that only a core-shell flow rate ratio of 1:3 could provide the appropriate conditions of identical surface tension and viscoelastic force for both PDLLA and PLGA, resulting in a narrow size distribution of smooth spheres approximately 1  $\mu$ m in diameter and with a clear core-shell structure. When the core-shell flow rate ratio was increased or decreased, particles with ambiguous core-shell structure or without core-shell dimension were generated.

The results showed that the core-shell submicron-spheres obtained in this study achieved independent release kinetics of the two GFs, incorporated in different compartments, while maintaining GF activity. VEGF in the shell section was delivered with an initial burst release, and nearly 80% of VEGF was released within

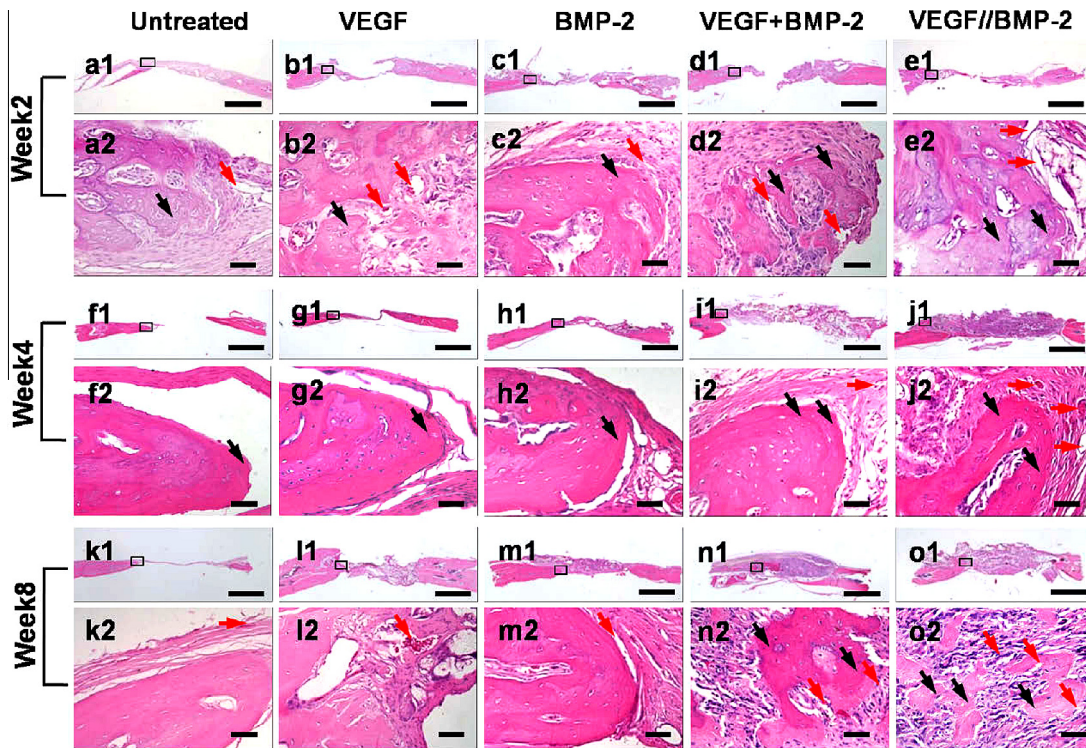


**Fig. 8.** Histological evaluation of defect repair at 2, 4, and 8 weeks after implantation at low (1.25 $\times$ ; bar = 2.5 cm) and high (40 $\times$ ; bar = 100 mm) magnification. Black arrows denote the nascent bone, red arrows denote the blood vessels. (For interpretation of the references to color in this figure legend, the reader is referred to the web version of this article.)

the first 10 days. Previous reports demonstrated that VEGF secretion takes place at the earlier healing stage after bone fracture [41], and the peak level of VEGF occurs between the 5th and the 10th day [13]. Thus, the VEGF release schema obtained in this study coincides with its physiological mode. BMP-2, which plays a pivotal role in bone regeneration, was produced throughout the fracture healing process. BMP-2 in the core of the spheres displayed relatively stable release behavior, as opposed to burst release. This is in good agreement with its physiological temporal pattern during bone defect healing [7]. The long-term sustained delivery can not only compensate for the fast degradation of BMP-2 in a complex local enzymatic environment, but also can avoid the heterotopic ossification, postoperative hematoma, and swelling caused by excessively high local dosage of BMP-2 [42]. Kempen et al. has reported that continuous release of BMP-2 enhanced ectopic osteogenic efficacy and improved in situ long bone defect repair [13]. These reports support our conclusion that the submicron scale core-shell spheres obtained in this study can serve as an effective carrier allowing controlled release of GFs at different kinetic rates. VEGF and BMP-2 are both hydrophilic proteins [43] that can rapidly diffuse into PBS medium. During the release period, VEGF in the shell was in direct contact with the PBS medium, so a burst release occurred according to predictions. The shell's chemical composition of PDLLA served as a barrier to slow the BMP-2 diffusion into the medium from the core. Thus, a sequential release of VEGF and BMP-2 was achieved. These sequential GF release profiles, mimicking their secretion events in nature bone repair [7,33], are considered a promising strategy for expediting GF-driven bone regenerative processes.

The amount of VEGF and BMP-2 used for bone regeneration ranged from several nanogram to more than 100 mg according to previous studies [7,13,28,35]. The bigger the experimental animals were, the more GFs were needed. Kempen et al. used about 2  $\mu$ g VEGF and 6–9  $\mu$ g BMP-2 to apply rat femoral defect implantation

and found that could improve bone healing [13]. So in this study 1.5  $\mu$ g VEGF and 3  $\mu$ g BMP-2 were set for each defect. The most appropriate amount of VEGF and BMP-2 and their ratio to result in the best bone regeneration would be studied in our future work.

Activity maintenance is another challenging issue in the delivery of GFs. The VEGF and BMP-2 released from PLGA/PDLLA core-shell submicron spheres were respectively found to enhance the proliferation of MECs and promote the osteogenic differentiation of BMSCs. MECs, specifically targeted by VEGF, are generally considered to form the lining layer of new blood vessels and play a key role in angiogenesis. BMSCs, critically sensitive to BMPs, have been well known to participate in osteogenesis by giving rise to a hierarchy of bone cell populations. Therefore, the delivery of VEGF and BMP-2 by core-shell submicron spheres might facilitate angiogenesis and osteogenesis in vivo and improve bone formation [3,14,44]. The bioactivity maintenance of GFs in this study could be ascribed to the favorable electrospaying technique, which is a one-step process that does not make use of potentially hazardous organic solvents or cross-linking agents. PDLLA and PLGA have been extensively used as biocompatible polymers, especially in drug delivery. No adverse effect has been reported on the bioactivity of the encapsulated GFs.

The collaborative effect of the dual delivery of VEGF and BMP-2 by various composite scaffolds has been explored to enhance endochondral bone regeneration through promoting angiogenesis [14]. However, in intramembranous bone defect repair, the coordinated associations between angiogenesis and intramembranous osteogenesis are still poorly understood. Therefore, the rat cranial bone defect model, where it is universally accepted that regeneration occurs through intramembranous ossification, was selected here to investigate how sequential VEGF and BMP-2 delivery from core-shell spheres influenced the coupling of angiogenesis-osteogenesis in intramembranous bone regeneration. Micro-CT showed that the quality and quantity of new bone formed in the

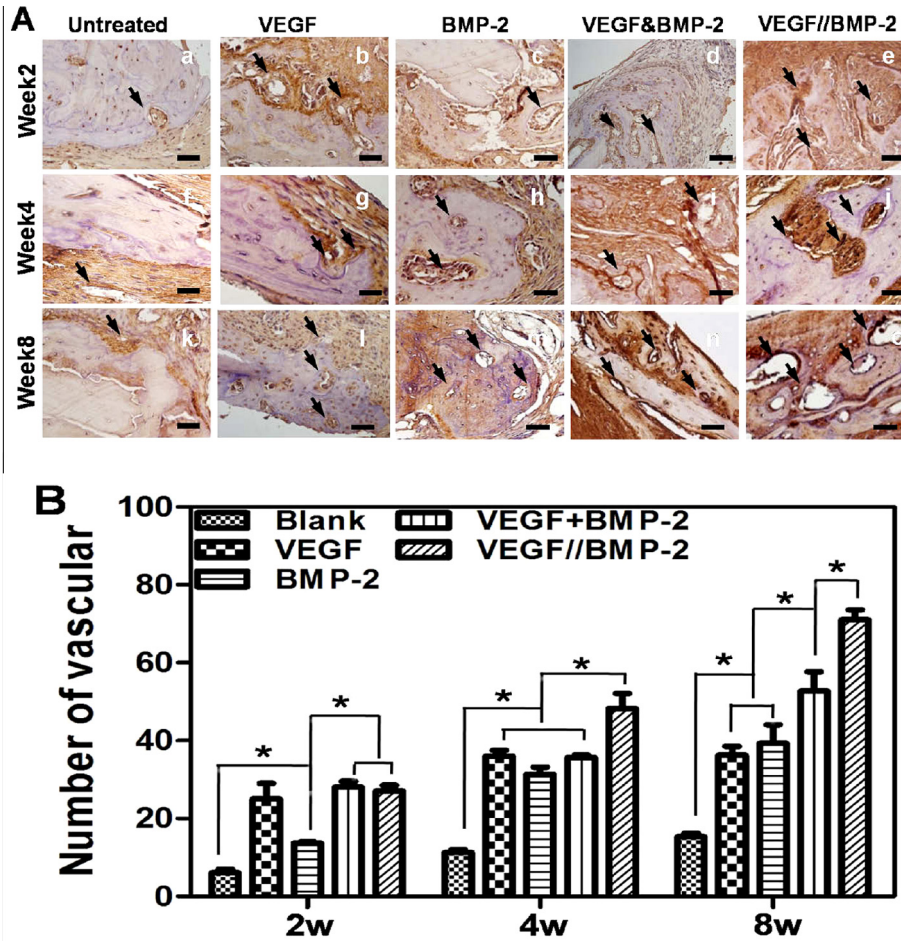


Fig. 9. Immunohistological staining of CD-31 after implantation of 2, 4, and 8 weeks (A), quantitative analysis of the area of vascular sections (B). The arrows denote the newly formed blood vessels; values represent mean ± SD (n = 3, \*p < 0.05).

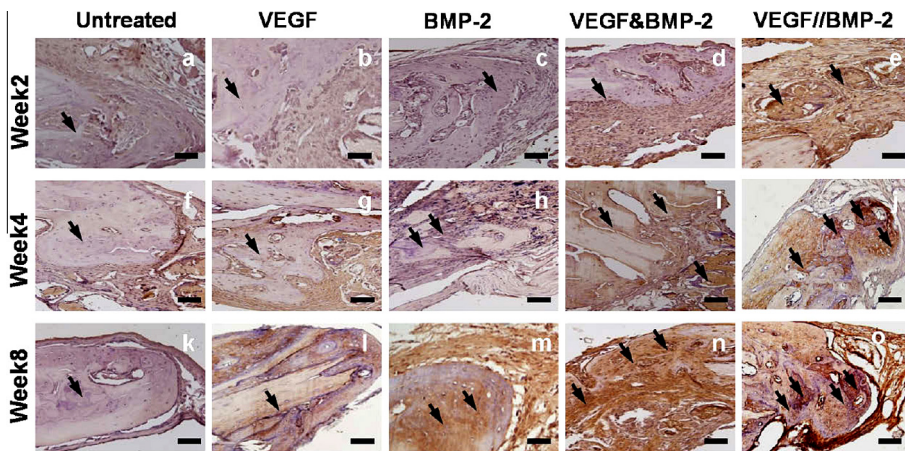


Fig. 10. Immunohistological staining of OCN in rat calvarial defects. The arrows denote the positive expression of OCN. Scale bar = 100 μm.

group PLGA–BMP-2/PDLLA–VEGF was superior to groups that released the GFs either individually or simultaneously, indicating the additive role of GFs in bone regeneration. Furthermore, the largest bone volume, most apparent by spicules in the central defect area, and the thickest bony trabeculae at bone defect peripheral sites, suggested that sequential delivery of VEGF and BMP-2 might

act in a time-dependent synergistic manner to regenerate bone tissue. Kempen et al. also found that the GFs would maintain a longer release time from about 1 month in vitro to 2 months in vivo [13]. This result was consistent with our findings. The main cause of this result could be the different release environment. Fluid for GFs to dissolve in and diffuse was less and flow slower when in vivo.

These results were consistent with previous reports, which proposed that sequential release of angiogenic and osteogenic biomolecules might replicate their temporal production during natural bone defect healing and neonatal bone morphogenesis.

Histological examination further confirmed the synergistic efficacy of sequentially released VEGF and BMP-2 on coupling of angiogenesis and osteogenesis. Hematoxylin and eosin staining showed continuous vigorous bone formation coupled with more amounts of vessels growing at 2 and 4 weeks, and more mature marrow cavity at 8 weeks, in the PDLLA-VEGF/PLGA-BMP-2 group. This unique bone repair outcome implied that sequential release of VEGF and BMP-2 mimics the physiological sequence of angiogenesis and osteogenesis. The early release of VEGF could initiate quick angiogenesis, favoring mass transportation and mesenchymal condensation, following which the ossification and maturation of condensations could be accelerated by BMP-2 to complete the osteogenesis cascades. Immunohistological staining showed the highest level of CD31 expression in the sequential release group at 2 and 4 weeks. It has been reported that CD31 positive endothelial cells have the ability to enhance osteogenic differentiation of perivascular osteoprogenitors through the Noggin angiocrine factor [45]. This endothelial-cell-specific and cell-autonomous Notch activity was proved to regulate bone angiogenesis and couple it to osteogenesis. In turn, the BMP-2 could also drive osteoprogenitor cells to secrete angiogenic factors such as VEGF and FGF to facilitate vascularization. As such, a virtuous cycle seems to be established by sequential release of VEGF and BMP-2, maintaining vessel in-growth and mesenchymal condensation ossification in pace with each other to yield preferable bone repair. Taken together, the synergistic effect of sequential VEGF and BMP-2 release to promote a time-dependent cycle of angiogenesis and osteogenesis contributes to bone regeneration.

## 5. Conclusion

In this study, PLGA-BMP-2/PDLLA-VEGF core-shell spheres, with VEGF in the outer layer and BMP-2 in the core, around 1  $\mu\text{m}$  in diameter, were successfully fabricated by a modified coaxial electrospinning technique. Sequential delivery consisting of an initial burst release of VEGF and a stable release of BMP-2 were achieved by these spheres. The released VEGF and BMP-2 maintained their bioactivity, and respectively enhanced the proliferation of endothelial cells and promoted the osteogenic differentiation of BMSCs. New bone formation, accompanied by abundant in-growth of blood vessels, was obtained by PLGA-BMP-2/PDLLA-VEGF submicron spheres implantation in vivo. These findings provided new evidence to elucidate the temporal orchestration of angiogenesis and osteogenesis, and to aid further development of novel bone regenerative scaffolds.

## Acknowledgments

The authors acknowledge the National Basic Research Program of China (No. 2012CB933900), the National Natural Science Foundation of China (Nos. 81171000, 51302005), the Beijing Natural Science Foundation (7144256, 7144257), the Beijing Nova Program (No. Z14111000180000).

## References

- [1] B.L. Eppley, W.S. Pietrzak, M.W. Blanton, Allograft and alloplastic bone substitutes: a review of science and technology for the craniomaxillofacial surgeon, *J. Craniofac. Surg.* 16 (6) (2005) 981–989. 2005-11-01.
- [2] B. Rinker, K.S. Vyas, Clinical applications of autografts, conduits, and allografts in repair of nerve defects in the hand: current guidelines, *Clin. Plast. Surg.* 41 (3) (2014) 533–550. 2014-07-01.
- [3] A. Hernandez, R. Reyes, E. Sanchez, M. Rodriguez-Evora, A. Delgado, C. Evora, In vivo osteogenic response to different ratios of BMP-2 and VEGF released from a biodegradable porous system, *J. Biomed. Mater. Res. A* 100 (9) (2012) 2382–2391. 2012-09-01.
- [4] L. Polo-Corrales, M. Latorre-Esteves, J.E. Ramirez-Vick, Scaffold design for bone regeneration, *J. Nanosci. Nanotechnol.* 14 (1) (2014) 15–56. 2014-01-01.
- [5] S.Y. Jeon, J.S. Park, H.N. Yang, D.G. Woo, K.H. Park, Co-delivery of SOX9 genes and anti-Cbfa-1 siRNA coated onto PLGA nanoparticles for chondrogenesis of human MSCs, *Biomaterials* 33 (17) (2012) 4413–4423. 2012-06-01.
- [6] Z.S. Patel, S. Young, Y. Tabata, J.A. Jansen, M.E. Wong, A.G. Mikos, Dual delivery of an angiogenic and an osteogenic growth factor for bone regeneration in a critical size defect model, *Bone* 43 (5) (2008) 931–940. 2008-11-01.
- [7] M. Mehta, K. Schmidt-Bleek, G.N. Duda, D.J. Mooney, Biomaterial delivery of morphogens to mimic the natural healing cascade in bone, *Adv. Drug Deliv. Rev.* 64 (12) (2012) 1257–1276. 2012-09-01.
- [8] R.E. Guldberg, Spatiotemporal delivery strategies for promoting musculoskeletal tissue regeneration, *J. Bone Miner. Res.* 24 (9) (2009) 1507–1511. 2009-09-01.
- [9] R.S. Carvalho, T.A. Einhorn, W. Lehmann, C. Edgar, A. Al-Yamani, A. Apazidis, et al., The role of angiogenesis in a murine tibial model of distraction osteogenesis, *Bone* 34 (5) (2004) 849–861. 2004-05-01.
- [10] H.P. Gerber, T.H. Vu, A.M. Ryan, J. Kowalski, Z. Werb, N. Ferrara, VEGF couples hypertrophic cartilage remodeling, ossification and angiogenesis during endochondral bone formation, *Nat. Med.* 5 (6) (1999) 623–628. 1999-06-01.
- [11] M.L. Brandi, P. Collin-Osdoby, Vascular biology and the skeleton, *J. Bone Miner. Res.* 21 (2) (2006) 183–192. 2006-02-01.
- [12] C.J. Percival, J.T. Richtsmeier, Angiogenesis and intramembranous osteogenesis, *Dev. Dyn.* 242 (8) (2013) 909–922. 2013-08-01.
- [13] D.H. Kempen, L. Lu, A. Heijink, T.E. Hefferan, L.B. Creemers, A. Maran, et al., Effect of local sequential VEGF and BMP-2 delivery on ectopic and orthotopic bone regeneration, *Biomaterials* 30 (14) (2009) 2816–2825. 2009-05-01.
- [14] B. Behr, M. Sorkin, M. Lehnhardt, A. Renda, M.T. Longaker, N. Quarto, A comparative analysis of the osteogenic effects of BMP-2, FGF-2, and VEGFA in a calvarial defect model, *Tissue Eng. Part A* 18 (9–10) (2012) 1079–1086. 2012-05-01.
- [15] T. Okuda, K. Tominaga, S. Kidoaki, Time-programmed dual release formulation by multilayered drug-loaded nanofiber meshes, *J. Control. Release* 143 (2) (2010) 258–264. 2010-04-19.
- [16] M.B. de Matos, A.P. Piedade, C. Alvarez-Lorenzo, A. Concheiro, M.E. Braga, H.C. de Sousa, Dexamethasone-loaded poly(epsilon-caprolactone)/silica nanoparticles composites prepared by supercritical CO<sub>2</sub> foaming/mixing and deposition, *Int. J. Pharm.* 456 (2) (2013) 269–281. 2013-11-18.
- [17] N. Amini, S. Mazinani, S.O. Ranaei-Siadat, M.R. Kalaei, S. Hormozi, K. Niknam, et al., Acetylcholinesterase immobilization on polyacrylamide/functionalized multi-walled carbon nanotube nanocomposite nanofibrous membrane, *Appl. Biochem. Biotechnol.* 170 (1) (2013) 91–104. 2013-05-01.
- [18] M.W. Chang, E. Stride, M. Edirisinghe, A new method for the preparation of monoporous hollow microspheres, *Langmuir* 26 (7) (2010) 5115–5121. 2010-04-06.
- [19] C. Borselli, F. Ungaro, O. Oliviero, I. D'Angelo, F. Quaglia, M.I. La Rotonda, et al., Bioactivation of collagen matrices through sustained VEGF release from PLGA microspheres, *J. Biomed. Mater. Res. A* 92 (1) (2010) 94–102. 2010-01-01.
- [20] Q. Xu, S.E. Chin, C.H. Wang, D.W. Pack, Mechanism of drug release from double-walled PDLLA(PLGA) microspheres, *Biomaterials* 34 (15) (2013) 3902–3911. 2013-05-01.
- [21] B. Li, T. Yoshii, A.E. Hafeman, J.S. Nyman, J.C. Wenke, S.A. Guelcher, The effects of rhBMP-2 released from biodegradable polyurethane/microsphere composite scaffolds on new bone formation in rat femora, *Biomaterials* 30 (35) (2009) 6768–6779. 2009-12-01.
- [22] D.H. Choi, R. Subbiah, I.H. Kim, D.K. Han, K. Park, Dual growth factor delivery using biocompatible core-shell microcapsules for angiogenesis, *Small* 9 (20) (2013) 3468–3476. 2013-10-25.
- [23] L. Cao, J. Luo, K. Tu, L.Q. Wang, H. Jiang, Generation of nano-sized core-shell particles using a coaxial tri-capillary electrospinning-removal method, *Colloids Surf. B Biointerfaces* 115 (2014) 212–218. 2014-03-01.
- [24] M. Mehta, K. Schmidt-Bleek, G.N. Duda, D.J. Mooney, Biomaterial delivery of morphogens to mimic the natural healing cascade in bone, *Adv. Drug Deliv. Rev.* 64 (12) (2012) 1257–1276.
- [25] S. Mitragotri, J. Lahann, Physical approaches to biomaterial design, *Nat. Mater.* 8 (1) (2009) 15–23. 2009-01-01.
- [26] C. Blüm, T. Scheibel, Control of drug loading and release properties of spider silk sub-microparticles, *BioNanoScience* 2 (2) (2012) 67–74.
- [27] B. Liu, H.M. Earl, D. Baban, M. Shoaibi, A. Fabra, D.J. Kerr, et al., Melanoma cell lines express VEGF receptor KDR and respond to exogenously added VEGF, *Biochem. Biophys. Res. Commun.* 217 (3) (1995) 721–727. 1995-12-26.
- [28] L. Wang, Y. Huang, K. Pan, X. Jiang, C. Liu, Osteogenic responses to different concentrations/ratios of BMP-2 and bFGF in bone formation, *Ann. Biomed. Eng.* 38 (1) (2010) 77–87. 2010-01-01.
- [29] K.J. Livak, T.D. Schmittgen, Analysis of relative gene expression data using real-time quantitative PCR and the 2(-Delta Delta C(T)) Method, *Methods* 25 (4) (2001) 402–408. 2001-12-01.
- [30] Y. Wang, X. Yang, W. Liu, F. Zhang, Q. Cai, X. Deng, Controlled release behaviour of protein-loaded microparticles prepared via coaxial or emulsion electrospinning, *J. Microencapsul.* 30 (5) (2013) 490–497. 2013-01-20.

- [31] A.P. Kusumbe, S.K. Ramasamy, R.H. Adams, Coupling of angiogenesis and osteogenesis by a specific vessel subtype in bone, *Nature* 507 (7492) (2014) 323–328. 2014-03-20.
- [32] X. Li, J. Wang, G. Su, Z. Zhou, J. Shi, L. Liu, et al., Spatiotemporal control over growth factor delivery from collagen-based membrane, *J. Biomed. Mater. Res. A* (2011) 11–14. 2011-11-14.
- [33] Y.C. Huang, D. Kaigler, K.G. Rice, P.H. Krebsbach, D.J. Mooney, Combined angiogenic and osteogenic factor delivery enhances bone marrow stromal cell-driven bone regeneration, *J. Bone Miner. Res.* 20 (5) (2005) 848–857. 2005-05-01.
- [34] H. Zhu, D. Yu, Y. Zhou, C. Wang, M. Gao, H. Jiang, et al., Biological activity of a nanofibrous barrier membrane containing bone morphogenetic protein formed by core-shell electrospinning as a sustained delivery vehicle, *J. Biomed. Mater. Res. B Appl. Biomater.* 101 (4) (2013) 541–552. 2013-05-01.
- [35] S. Suzuki, T.A. Asoh, A. Kikuchi, Design of core-shell gel beads for time-programmed protein release, *J. Biomed. Mater. Res. A* 101 (5) (2013) 1345–1352. 2013-05-01.
- [36] Y. Yang, X. Li, W. Cui, S. Zhou, R. Tan, C. Wang, Structural stability and release profiles of proteins from core-shell poly (DL-lactide) ultrafine fibers prepared by emulsion electrospinning, *J. Biomed. Mater. Res. A* 86 (2) (2008) 374–385. 2008-08-01.
- [37] X. Li, P. Du, P. Liu, Novel biocompatible pH-stimuli responsive superparamagnetic hybrid hollow microspheres as tumor-specific drug delivery system, *Colloids Surf. B Biointerfaces* 122C (2014) 99–106. 2014-07-01.
- [38] N. Arya, S. Chakraborty, N. Dube, D.S. Katti, Electrospinning: a facile technique for synthesis of chitosan-based micro/nanospheres for drug delivery applications, *J. Biomed. Mater. Res. B Appl. Biomater.* 88 (1) (2009) 17–31. 2009-01-01.
- [39] D. Gupta, J. Venugopal, S. Mitra, D.V. Giri, S. Ramakrishna, Nanostructured biocomposite substrates by electrospinning and electrospinning for the mineralization of osteoblasts, *Biomaterials* 30 (11) (2009) 2085–2094. 2009-04-01.
- [40] H. Valo, L. Peltonen, S. Vehvilainen, M. Karjalainen, R. Kostianen, T. Laaksonen, et al., Electrospay encapsulation of hydrophilic and hydrophobic drugs in poly(L-lactic acid) nanoparticles, *Small* 5 (15) (2009) 1791–1798. 2009-08-03.
- [41] J.M. Kanczler, R.O. Oreffo, Osteogenesis and angiogenesis: the potential for engineering bone, *Eur. Cell Mater.* 15 (2008) 100–114. 2008-01-20.
- [42] B. Perri, M. Cooper, C. Laurysen, N. Anand, Adverse swelling associated with use of rh-BMP-2 in anterior cervical discectomy and fusion: a case study, *Spine J.* 7 (2) (2007) 235–239. 2007-03-01.
- [43] J. Patterson, R. Siew, S.W. Herring, A.S. Lin, R. Guldberg, P.S. Stayton, Hyaluronic acid hydrogels with controlled degradation properties for oriented bone regeneration, *Biomaterials* 31 (26) (2010) 6772–6781. 2010-09-01.
- [44] C. Schmitt, R. Lutz, H. Doering, M. Lell, J. Ratky, K.A. Schlegel, Bio-Oss(R) blocks combined with BMP-2 and VEGF for the regeneration of bony defects and vertical augmentation, *Clin. Oral Implants Res.* 24 (4) (2013) 450–460. 2013-04-01.
- [45] S.K. Ramasamy, A.P. Kusumbe, L. Wang, R.H. Adams, Endothelial Notch activity promotes angiogenesis and osteogenesis in bone, *Nature* 507 (7492) (2014) 376–380. 2014-03-20.